

<https://doi.org/10.1038/s41528-024-00324-0>

Highly conductive polymer electrodes for polymer light-emitting diodes

Check for updates

Jin Xu^{1,2,3,5} ✉, Ke Du^{1,5}, Feng Peng⁴, Zhenzhong Sun^{1,3}, Zhiming Zhong¹, Weiji Feng¹ & Lei Ying^{2,4} ✉

Organic light-emitting diodes (OLEDs) offer the advantage of flexibility; however, the use of traditional transparent anode ITO limits further extension of their flexible characteristics. In this study, we propose employing a polymer polybenzodifuranedione (PBFDO) as a flexible transparent anode instead of the rigid ITO. To address the issue encountered during the PBFDO solution spin-coating process, we introduced n-butanol into the PBFDO conductive solution to reduce its viscosity and freezing point by modulating intermolecular hydrogen bonding interactions. Consequently, high-quality PBFDO films with high conductivity, superior transmittance, and low surface roughness were successfully obtained via spin-coating. Moreover, due to its proper work function, regular molecular stacking, and low refractive index properties, PBFDO electrode facilitate efficient carrier injection and transport as well as photon extraction. The resulting device utilizing a PBFDO anode combined with Super Yellow as the light-emitting layer exhibited excellent performance characteristics including a normal threshold voltage of 2.6 V and a maximum luminous efficiency of 12.8 cd A⁻¹ comparable to that device based on the ITO electrode. Furthermore, flexible device also achieved satisfactory performance (7.7 cd A⁻¹) when using the PEN substrate.

The organic light-emitting diode (OLED) demonstrates active luminescence, rapid response time, high contrast ratio, and exceptional flexibility, rendering it extensively utilized in the fields of display and lighting^{1–6}. The indium tin oxide (ITO) currently serves as the predominant transparent electrode in OLED devices, but its rigid properties imposes limitations on further extension of their flexible characteristics⁷. The development of flexible electrodes becomes imperative for the next generation of light-emitting display devices that can conform to human skin. Therefore, the research and development of flexible electrodes present a scientific challenge that necessitates resolution. The key characteristic of flexible electrode materials lies in their simultaneous requirement for high electrical conductivity and stretchability, which traditional metal or metal oxide electrodes solely exhibit the former without meeting the demands of future advancements.

Currently, the prevalent approach for fabricating flexible electrodes involves incorporating highly conductive materials such as silver nanowires, carbon nanotubes, and graphene into flexible substrates⁸. Among them, the silver nanowires, a one-dimensional nanomaterial possessing exceptional electrical conductivity and high light transmittance, are widely regarded as

the most promising substitute for traditional ITO transparent electrodes. The flexible electrode based on silver nanowires has been achieved through various measures, including in situ polymerization of elastomer onto the surface of silver nanowires and direct spin coating of elastomer solution onto the silver nanowire surface, ensuring their seamless integration into the elastomeric matrix^{9–13}. Due to the disparate material systems of silver nanowires and flexible polymers, their interface compatibility is limited, thereby compromising the long-term stability of electrode utilization.

In order to address these challenges, it is imperative to explore a highly conductive material that exhibits compatibility with flexibility. Undoubtedly, highly conductive polymers emerge as the most promising candidates; however, conventional conductive polymers such as polyaniline, polythiophene, poly(3,4-ethylenedioxythiophene)-poly(styrenesulfonate) (PEDOT: PSS), pose limitations in their direct utilization as flexible electrodes for OLED devices due to their relatively low conductivity. The conductivity and flexibility of PEDOT: PSS have been enhanced through various techniques, including acid treatment, incorporation of small molecule plasticizers, and topological supramolecule, thereby augmenting its potential for application in flexible electronics^{14–17}. Especially, Bao et al.

¹School of Mechanical Engineering, Dongguan University of Technology, Dongguan 523808, China. ²Institute of Polymer Optoelectronic Materials and Devices, State Key Laboratory of Luminescent Materials and Devices, South China University of Technology, Guangzhou 510640, China. ³Guangdong-Hong Kong-Macao Joint Laboratory for Neutron Scattering Science and Technology, Dongguan University of Technology, Dongguan 523808, China. ⁴Dongguan Volt-Amp Optoelectronics Technology Co. Ltd., Dongguan 523808, China. ⁵These authors contributed equally: Jin Xu, Ke Du. ✉e-mail: xujin@dgut.edu.cn; msleiyang@scut.edu.cn

successfully incorporated PEDOT: PSS into a topology-based polymer based on polyethylene glycol framework, resulting in highly oriented PEDOT molecules and achieving exceptional conductivity and stretchability of polymer electrodes¹⁶. The utilization of this polymer electrode has demonstrated its efficacy in fabricating intrinsic stretchable light-emitting diodes with satisfactory performance¹⁷.

Recently, the *n*-type self-doped conducting polymer, polybenzodifuranedione (PBFDO), which exhibits exceptional conductivity and possesses a suitable work function, has emerged as a promising candidate for replacing ITO as a flexible electrode^{18,19}. Compared to the commercially available highly conductive PEDOT: PSS (PH1000: 1000 S cm⁻¹), PBFDO exhibits more significant advantages in terms of conductivity. Nevertheless, prior to the direct utilization of commercial PBFDO conductive solutions for obtaining high-quality films through spin coating, it is imperative to address the following issues. The presence of hydrogen bonds between PBFDO polymer molecules results in elevated viscosity and even slight polymer precipitation within the solution. Consequently, when employing the spinning coating process to prepare PBFDO thin films, their quality is compromised, rendering them unsuitable as transparent electrodes for devices. Simultaneously, the high freezing point of DMSO solvent in PBFDO conductive solution poses challenges due to the solidification and precipitation of the PBFDO polymer within the conductive solution, thereby impacting its practical utilization¹⁹.

In order to address these issues, a specific proportion of *n*-butanol was incorporated into the PBFDO conductive solution to modulate intermolecular hydrogen bonding interactions. On one hand, the hydrogen bonding between *n*-butanol and PBFDO can impede the formation of hydrogen bonds among PBFDO molecules, thereby reducing the solution's viscosity. On the other hand, the interaction between *n*-butanol and DMSO molecules hinders the crystallization of DMSO and lowers the freezing point of the solution. By utilizing the modified PBFDO conductive solution, high-quality PBFDO films exhibiting high conductivity, superior transmittance, and low surface roughness were successfully fabricated via spin coating technique. The resulting device employing flexible PBFDO anode in conjunction with Super Yellow as a luminescent layer achieved comparable device efficiency to that based on ITO anodes.

Results and discussion

The commercial PBFDO solution (unmodified PBFDO solution) utilizes DMSO as the solvent, with its molecular formula depicted in Fig. 1. However, due to its propensity for solidification and precipitation, as well as its high viscosity, the film quality of the spinning-coated solution is compromised. By analyzing the molecular structure of PBFDO and DMSO, it was

found that the protonated hydrogen atoms in PBFDO readily form intermolecular hydrogen bonds with sulfoxide groups in DMSO and carbonyl groups in PBFDO²⁰. Evidently, the former's hydrogen bonding facilitates the solubility of PBFDO, whereas the latter's hydrogen bonding elevates solution viscosity and hampers PBFDO dissolution.

The Fourier Transform infrared (FTIR) spectrum of the PBFDO film (Fig. 2) clearly exhibits an absorption peak indicative of hydrogen bonding within the range of 3200–3550 cm⁻¹, thereby confirming the presence of intermolecular hydrogen bonds among PBFDO molecules²¹. Similarly, the FTIR spectra of a unmodified PBFDO solution also demonstrate an absorption peak characteristic of hydrogen bonding (3431 cm⁻¹). The addition of *n*-butanol to the PBFDO solution aims to regulate hydrogen bonding, reducing viscosity and freezing point while enhancing solution stability. The addition of *n*-butanol to the PBFDO conductive solution (modified PBFDO solution) leads to a broadening and downward shift of the hydrogen bonding infrared characteristic peak at 3392 cm⁻¹, possibly attributed to the involvement of *n*-butanol in facilitating hydrogen bond formation. As illustrated in Fig. 1, the hydroxyl group of *n*-butanol can also form intermolecular hydrogen bonds with sulfoxide groups in DMSO and carbonyl groups in PBFDO. To further validate the involvement of *n*-butanol in the aforementioned hydrogen bond formation, separate FTIR tests were conducted on *n*-butanol and a mixture solvent of *n*-butanol-DMSO. As depicted in Fig. 2, a distinct peak at 3333 cm⁻¹ indicates the presence of hydrogen bonding in *n*-butanol, whereas upon the addition of DMSO solvent, the characteristic hydrogen bond peak in the mixture solvent shifts to a higher wavenumber at 3380 cm⁻¹. This shift can be attributed to weak hydrogen bonding between the sulfoxide group and hydroxyl group²². Previous literature reports have also observed a characteristic hydrogen bond peak around 3360 cm⁻¹ between *n*-butanol and carbonyl groups²³. Based on these findings, we analyzed the hydrogen bond characteristic peaks in modified PBFDO solution through fitting processing (see Fig. 2b). The results confirm intermolecular hydrogen bonding interactions between *n*-butanol and both DMSO and PBFDO due to the corresponding absorption peak at 3380 cm⁻¹ and 3360 cm⁻¹.

On one hand, due to directionality inherent to hydrogen bonding, *n*-butanol forms intermolecular hydrogen bonding with DMSO which disrupts crystallization processes among DMSO molecules and reduces freezing point for this system^{24,25}. By incorporating *n*-butanol, the addition of this compound leads to a substantial reduction in the freezing point of the conductive solution from -1 °C to -27 °C according to the Differential Scanning Calorimetry (DSC) data (Fig. 3a), thereby significantly bolstering its cryogenic resistance. The inner illustration in Fig. 3a depicts the phenomenon observed after subjecting both the modified and unmodified

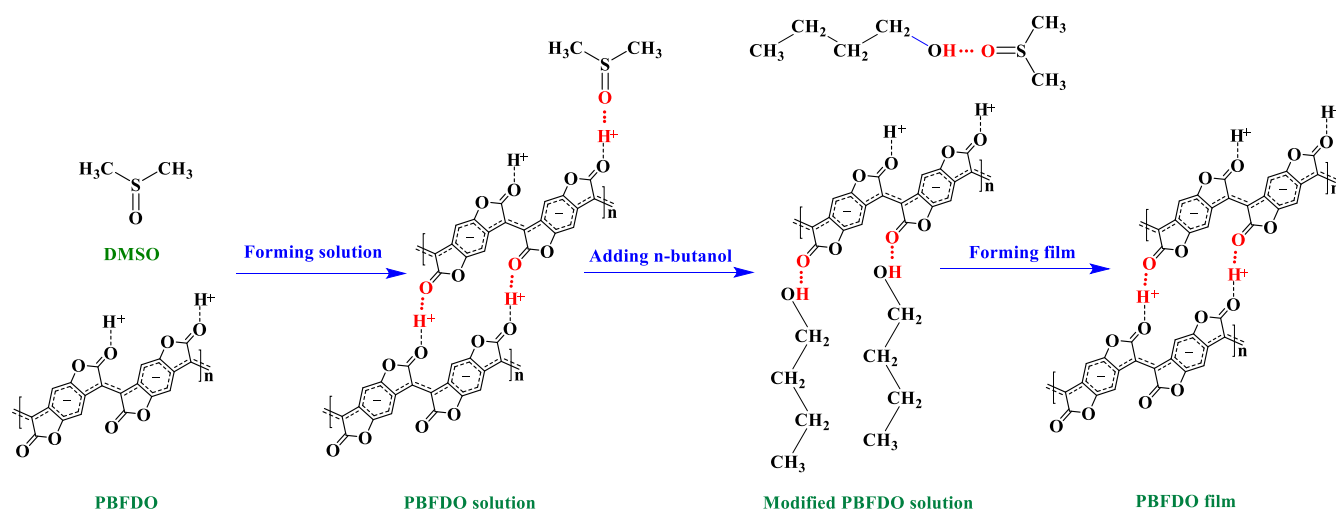


Fig. 1 | Chemical structure and intermolecular hydrogen bonds of materials. Chemical formulas of PBFDO, DMSO, and *n*-butanol along with a schematic diagram illustrating the potential intermolecular hydrogen bond between them.

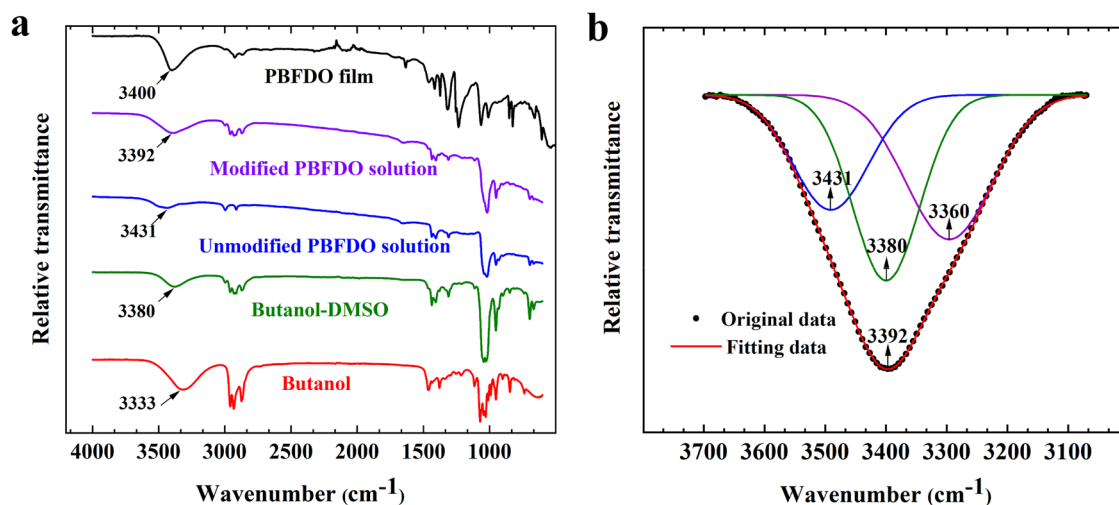


Fig. 2 | FTIR spectra of relevant materials. **a** FTIR spectra of the PBFD0 film, relative solvent and solution. **b** Fitting data of hydrogen bond characteristic absorption peaks of modified PBFD0 solution.

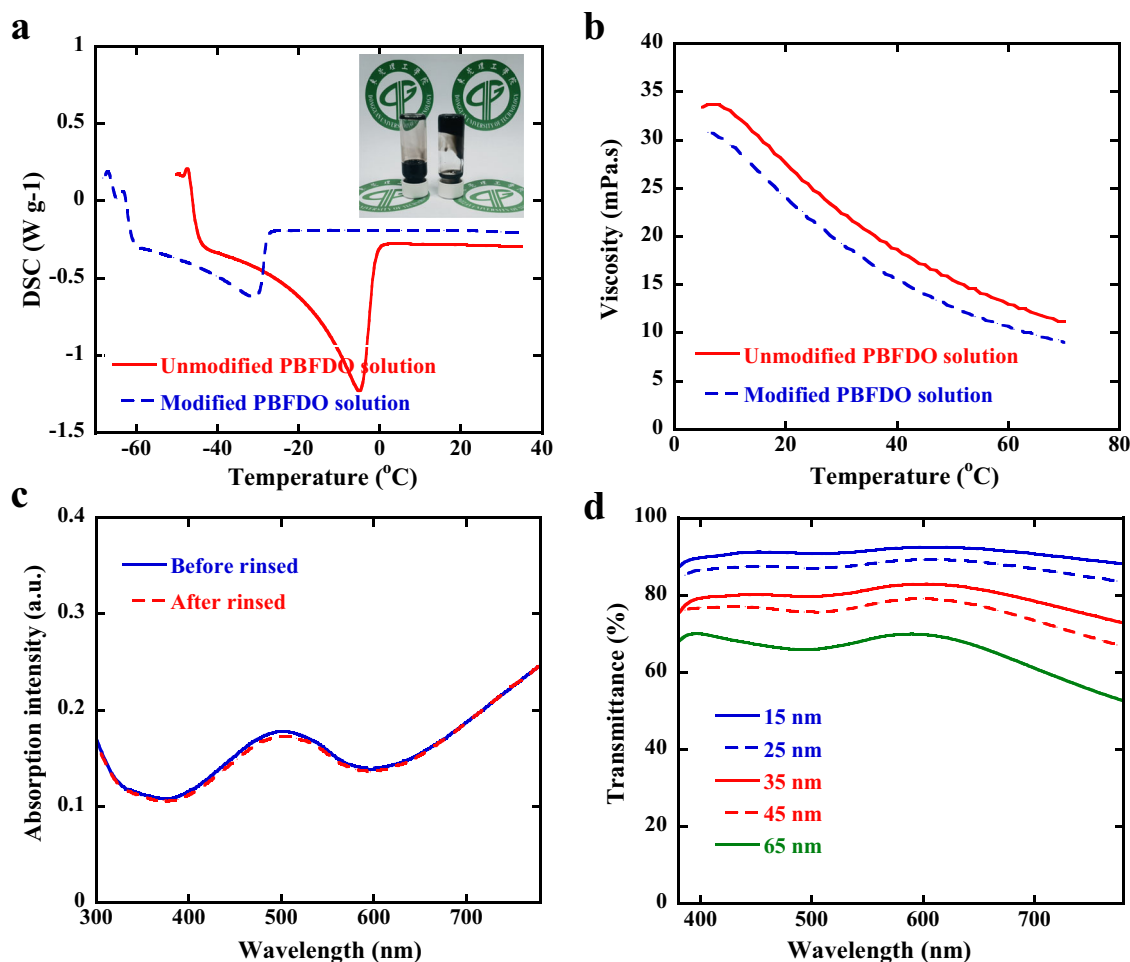


Fig. 3 | Freezing point, viscosity, solvent resistance, and optical transmittance of PBFD0 solution and PBFD0 film. **a** Differential scanning calorimetry (DSC) and **(b)** viscosity-temperature profiles were obtained for unmodified and modified

PBFD0 solutions using n-butanol as a modifier. **c** Absorption spectra of PBFD0 films before and after rinsing with DMSO. **d** Transmittance of PBFD0 films with air as the base at varying thicknesses.

PBFD0 solutions to a temperature of -15°C in a refrigerator for 4 h simultaneously. Evidently, the left bottle represents the modified PBFD0 solution, which remains in its liquid state, while the right bottle portrays the completely frozen unmodified solution. On other hand, hydrogen bonding

is saturated, and the formation of a hydrogen bond between n-butanol and PBFD0 will diminish the occurrence of hydrogen bonds among PBFD0 molecules, thereby reducing solution viscosity and enhancing solution stability. To further investigate changes in viscosity, the temperature-

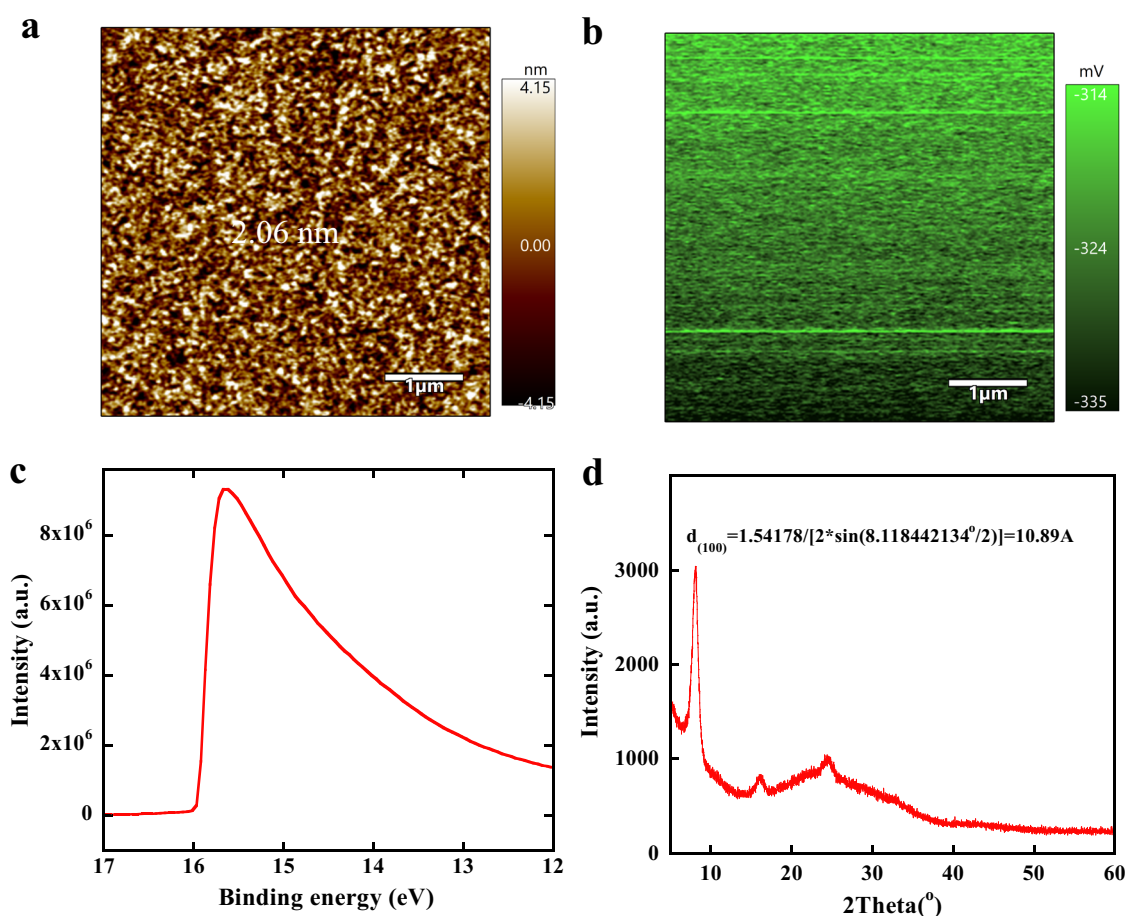


Fig. 4 | Analysis of the surface morphology, work function, and crystallization of PBFDO film. **a** AFM surface topography, **(b)** surface electrostatic potential, **(c)** Ultraviolet photoelectron spectrum, and **(d)** XRD characteristics of the PBFDO film.

dependent viscosity curves were measured based on the unmodified and modified PBFDO solution. What needs to be pointed out is that the unmodified PBFDO solution was diluted with an equal volume of DMSO to minimize solvent dilution effects. As shown in Fig. 3b, both solutions exhibit a significant decrease in viscosity with increasing temperature due to enhanced molecular thermal motion and weakened intermolecular forces. Moreover, it is evident from the Fig. 3b that the viscosity of the modified PBFDO solution is approximately 4 mPa.s lower than that of the unmodified counterpart at identical temperatures. The reduction in solution viscosity facilitates filtration treatment of the filter membrane and enhances film quality when prepared using spin-coating method.

In addition, as depicted in Supplementary Fig. 1, when equal volumes (15 μ L) of unmodified and modified PBFDO solutions are dropped onto a glass substrate, it can be observed that the unmodified PBFDO solution exhibits aggregation at the center of the glass substrate, whereas the modified PBFDO solution demonstrates near-complete coverage on the surface of the glass substrate. Evidently, spin coating is more favorably facilitated by the modified PBFDO solution.

The absorption intensity of the PBFDO film remained essentially unaltered upon rinsing with DMSO, as depicted in Fig. 3c. This observation suggests that PBFDO exhibits limited solubility in DMSO when forming thin films, likely attributed to its robust intermolecular hydrogen bonding forces. Thus, as illustrated in Supplementary Fig. 2, PBFDO films were fabricated with thicknesses ranging from 15 nm to 65 nm through multiple spin coating techniques. The corresponding transmittance was measured using a UV-visible spectrophotometer as depicted in Fig. 3d. Notably, the average transmittance of the PBFDO conductive film with a thickness of 15 nm reached an impressive value of 91% within the visible range

(380–780 nm). However, when increasing the thickness to 25 nm, there was a slight decrease in transmittance to approximately 87%. Further increasing the thickness to values between 35–45 nm resulted in transmittance levels ranging from 76% to 80%. Consequently, it can be inferred that for applications requiring transparent electrodes in light-emitting devices, PBFDO films with a thickness below 30 nm are particularly suitable.

The Supplementary Fig. 3 demonstrates a defect-free and smooth surface of the PBFDO film by spin-coating. Subsequent atomic force microscopy (AFM) analysis revealed uniform polymer dispersion, with an exceptionally low surface roughness of 2.06 nm (Fig. 4a). This smooth surface facilitates reduced leakage current in devices, making it suitable for transparent conducting electrode.

Meanwhile, the work function of the PBFDO film was also determined using scanning kelvin probe force microscopy (SKPM). In order to mitigate the impact of probe oxidation and surface contamination on its work function, we employed highly oriented pyrolytic graphite (HOPG) with a known work function of 4.6 eV as the reference sample for evaluating and characterizing the work function of PBFDO films²⁶. Figure 4b illustrates the surface potential image of the PBFDO film, exhibiting an average value of approximately -0.324 V. By employing the following formula²⁷,

$$WF_{PBFDO} = WF_{HOPG} - e(V_{PBFDO} - V_{HOPG}) \quad (1)$$

We have determined that the work function of PBFDO is 5.32 eV based on the recorded V_{HOPG} value of 0.395 V. In addition, the work function of PBFDO thin film also was analyzed via ultraviolet photoelectron spectroscopy (UPS), yielding a calculated value of 5.33 eV that is highly consistent with the SKPM results (Fig. 4c). However, it should be noted that this value

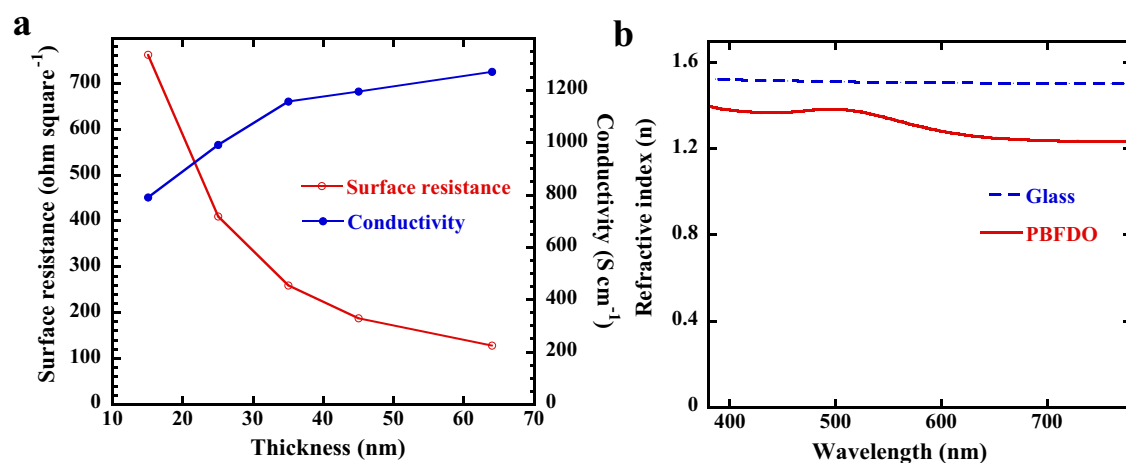


Fig. 5 | Conductivity and refractive index of PBFDO film. **a** Relationship curve between the conductivity and surface resistance of PBFDO thin films on a glass substrate as a function of film thickness. **b** Refractive index of PBFDO film and glass in the visible light region.

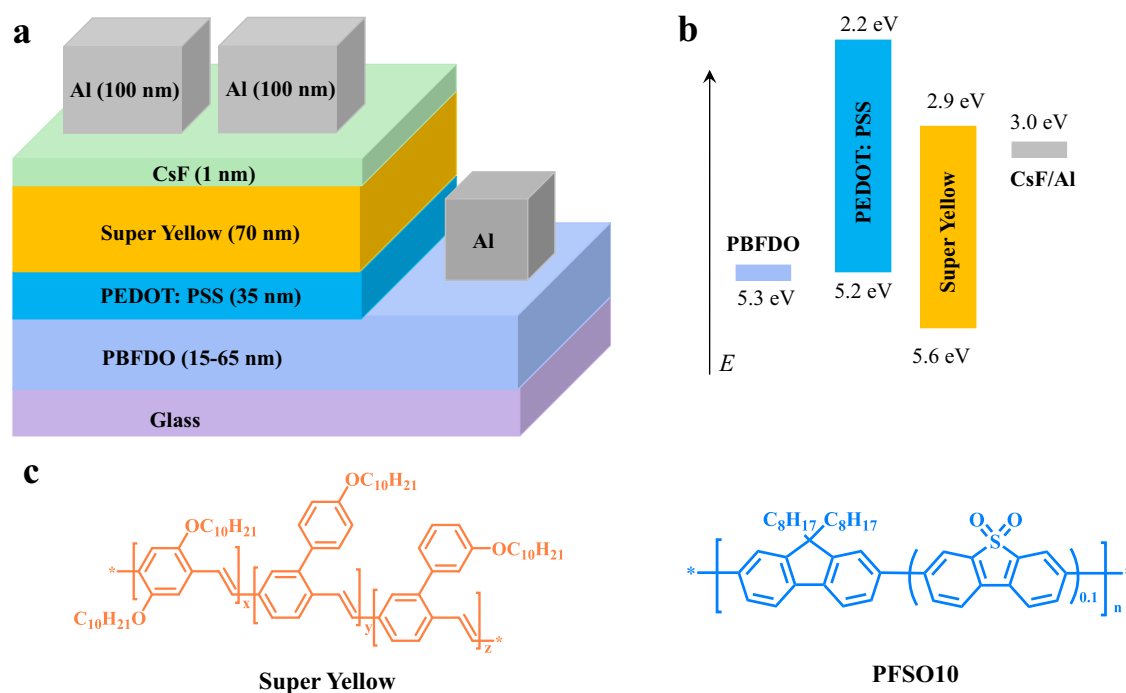


Fig. 6 | Device structure and corresponding energy level alignment. **a** Schematic representation of the OLED device structure incorporating a PBFDO bottom electrode and **(b)** its corresponding energy level alignment. **c** Chemical structure of the light emitting polymer Super Yellow (SY) and poly(9,9-dioctyl-2,7-fluorene-co-3,7-dibenzothiophene-S,S-dioxide) (PFSO10).

deviates from the previously reported work function of PBFDO¹⁸, which may be attributed to various factors such as variations in test substrates, film thicknesses, and oxygen adsorption^{28,29}.

The film's crystallization information was also characterized using X-ray diffraction (XRD), as depicted in Fig. 4d. The PBFDO film exhibited a prominent crystallization peak on the (100) surfaces, with a corresponding layer spacing of 10.89 Å, which aligns well with previously reported findings¹⁸. The aforementioned observation highlights the fact that spin-coated PBFDO films exhibit a highly regular molecular stacking morphology, which can be attributed to their unique molecular structure characterized by the absence of side chains and the presence of a rigid main chain structure. Consequently, this structural feature facilitates efficient charge transport.

As an electrode, possessing excellent electrical conductivity is imperative; therefore, the surface resistance and conductivity of the PBFDO

films with varying thicknesses were measured using a four-probe conductivity tester (Fig. 5a). At a PBFDO thickness of 15 nm, the surface resistance was measured to be 763 ohm square⁻¹, which exhibited a significant reduction to 410.2 ohm square⁻¹ upon increasing the thickness to 25 nm. Subsequently augmenting the PBFDO thickness led to a continuous decline in surface resistance, reaching its minimum value of 128 ohm square⁻¹ at a thickness of 65 nm. Correspondingly, the electrical conductivity demonstrated an increase from 790 S cm⁻¹ to 1271 S cm⁻¹.

The refractive index of the PBFDO film and glass substrate was determined using an ellipsometer. As depicted in Fig. 5b, within the visible region, the refractive index (n) of the PBFDO film exhibited a decreasing trend as the wavelength increased, consistently ranging between 1.23 and 1.40, while that of glass substrate was approximately 1.51. As commonly acknowledged, when light propagates across the interface between different

Table 1 | Key performance parameters of electrodes and devices

Thickness (nm)	Key performance of electrodes			Key performance of devices				
	Surface resistance (ohm square ⁻¹)	Conductivity (S cm ⁻¹)	^a Transmittance (%)	WF (eV)	^b V _{th} (V)	LE _{max} (cd A ⁻¹)	L _{max} (cd m ⁻²)	^c CIE (x, y)
PBFDO	128	1271	65	5.3	2.6	7.2	24,324	(0.47, 0.52)
	188	1195	76		2.6	11.0	18,354	(0.46, 0.53)
	259	1157	80		2.6	11.0	14,095	(0.46, 0.53)
	410	991	87		2.6	12.8	9598	(0.46, 0.53)
	763	790	91		2.6	11.1	2351	(0.47, 0.52)
ITO	15	3704	90	4.8	2.6	13.5	124,804	(0.48, 0.51)
	45	3174	90		2.6	13.7	104,109	(0.46, 0.53)
	110	3030	97		2.6	13.1	77,276	(0.47, 0.53)
	450	2220	98		2.6	12.7	28,248	(0.47, 0.53)

^aAverage transmittance in the visible region using air as a base.^bDefined as the voltage at a luminance of 1 cd m⁻².^cColor coordinates measured at J = 10 mA cm⁻².

media, it exhibits transmission, refraction, and reflection phenomena. Evidently, the processes of transmission and refraction facilitate the extraction of light, whereas reflection impedes its extraction. It is important to note that total reflection occurs when light is incident from an optically dense medium to an optically sparse medium at an incident angle exceeding a specific critical angle. The critical angle of total reflection, denoted as θ , is determined by the refractive indices of optically sparse (n_1) and optically dense (n_2) media, and it satisfies the following equation:

$$\sin \theta = \frac{n_1}{n_2} \quad (2)$$

Based on the conventional ITO conductive glass, the critical angle of total light reflection from ITO ($n_2 = 1.85$) into the glass ($n_1 = 1.51$) can be calculated as 55° . As shown in Supplementary Fig. 4a, refracted light will be unable to penetrate the glass substrate when incident light enters the glass at an angle exceeding 55° . In contrast, the absence of total reflection is observed in the glass/PBFDO electrode configuration due to PBFDO's lower refractive index compared to that of the glass substrate (Supplementary Fig. 4b). As a result, this circumvents any loss in light caused by total reflection and enhances the overall efficiency of light extraction.

As depicted in Fig. 6a, based on the highly conductive PBFDO electrode and luminous polymer super yellow (SY), the devices with a configuration of Glass/PBFDO/PEDOT: PSS/SY/CsF/Al were fabricated. The PBFDO electrode possesses an energy level that aligns with PEDOT: PSS, thereby facilitating the efficient injection of hole carriers (Fig. 6b). The PEDOT: PSS can effectively block electron transport due to the large energy difference (0.7 eV).

Additionally, reference devices with ITO electrodes exhibiting different surface resistances (15 ohm square⁻¹, 45 ohm square⁻¹, 110 ohm square⁻¹ and 450 ohm square⁻¹) were also prepared. The corresponding key performance parameters of electrodes and devices are presented in Table 1, Fig. 7 and Supplementary Fig. 5. The devices exhibit a pronounced diode injection phenomenon, and the current density shows an increasing trend with the growth of PBFDO thickness owing to the enhanced electrical conductivity (Fig. 7a). Similarly, the ITO reference device exhibited a similar trend (Supplementary Fig. 5a).

As shown in Table 1, all of the devices have the same threshold voltage (V_{th}) of 2.6 V indicating unobstructed carrier injection. Moreover, the maximum luminous efficiency (LE_{max}) of the device shows minimal correlation with the conductivity of the electrode, while the maximum luminance (L_{max}) decreases with decreasing conductivity. The optimized device based on the PBFDO electrode (25 nm) achieved a LE_{max} of 12.8 cd A⁻¹ comparable to ITO reference device (12.7 cd A⁻¹) with similar surface resistance (450 ohm square⁻¹). However, the L_{max} of the devices based on the PBFDO electrode is relatively low due to its comparatively lower conductivity. As shown in the Fig. 7d, an increase in PBFDO thickness results in initially narrower EL spectra followed by broadening which can be attributed to microcavity effects^{31,32}.

Based on the optimal thickness (25 nm) for PBFDO, a flexible device was fabricated using polyethylene naphthalate (PEN) as the substrate, the corresponding device data are presented in the Table 2 and Supplementary Fig. 6. The digital photograph of the device in its bent lighting state is depicted in the last column of Table 2, demonstrating the device's remarkable flexibility when subjected to bending. The V_{th} of the flexible device also measures 2.6 V, exhibiting a LE_{max} of 7.7 cd A⁻¹ and a L_{max} of 4078 cd cm⁻². The relatively lower efficiency could be attributed to the lower light transmittance (approximately 82%) and limited light extraction efficiency of the PEN substrate.

Considering the negligible hole injection barrier between the PBFDO (WF: 5.3 eV) and the SY (HOMO: 5.6 eV)³³, we endeavored to eliminate PEDOT:PSS layer to fabricate a device with a simple configuration of Glass/PBFDO/SY/CsF/Al. In addition, we fabricated a reference device employing ITO electrode. As depicted in Table 2 and Supplementary Fig. 7, owing to the substantial hole injection barrier between ITO (4.8 eV) and SY (HOMO: 5.6 eV), device utilizing ITO electrode exhibited remarkably high V_{th} (4.4 V)

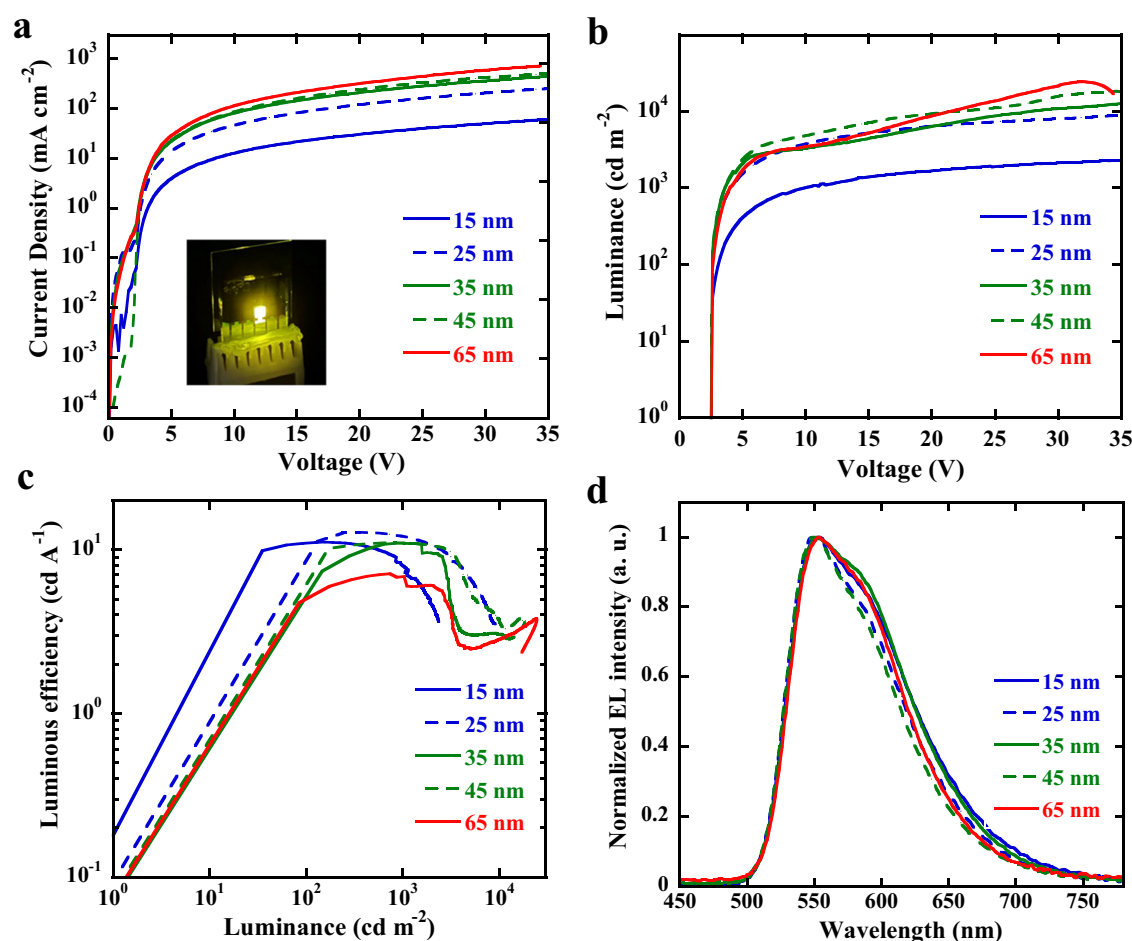

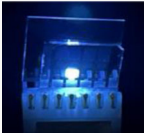


Fig. 7 | Device performance based on the PBFDO electrode. a Current density-voltage curves, (b) luminance-voltage curves, (c) luminous efficiency-luminance curves, and (d) EL spectra of devices utilizing PBFDO electrode with varying thicknesses.

Table 2 | Summary of key performance parameters of the devices

Device Structure	^a V _{th} (V)	LE _{max} (cd A ⁻¹)	L _{max} (cd m ⁻²)	^b CIE (x, y)	^c Digital Photograph
PEN/PBFDO/PEDOT: PSS/SY/CsF/Al	2.6	7.7	4078	(0.47, 0.52)	
Glass/PBFDO/SY/CsF/Al	2.6	5.1	14712	(0.47, 0.52)	
Glass/ITO/SY/CsF/Al	4.4	0.8	1844	(0.49, 0.51)	
Glass/PBFDO/PEDOT: PSS/PFSO10/CsF/Al	3.0	2.5	1717	(0.15, 0.13)	
Glass/ITO/PEDOT: PSS/PFSO10/CsF/Al	3.0	2.6	4392	(0.15, 0.14)	

^aDefined as the voltage at a luminance of 1 cd m⁻².

^bColor coordinates measured at J = 10 mA cm⁻².

^cDigital photograph of flexible device and the blue OLED utilizing the PBFDO electrode.

and low LE_{max} (0.8 cd A⁻¹). Conversely, due to the absence of any hole injection barrier, the device utilizing PBFDO electrode demonstrated a normal V_{th} (2.6 V) and moderate LE_{max} values of 5.1 cd A⁻¹ (Table 2).

The stability of the device, based on PBFDO electrode, is evaluated in terms of spectral stability and lifetime. On one hand, the EL spectrum of the device is measured at various applied voltages, and it exhibits remarkable stability within the voltage range of 4–20 V without any discernible alterations (Fig. 8a). On the other hand, we also investigated the luminance degradation curve of the device over time by measuring a device with an

initial brightness of 1000 cd m⁻² under ambient conditions. Notably, as illustrated in Fig. 8b, the operational lifetime of device utilizing PBFDO electrode is significantly extended compared to that employing ITO electrode. Even after continuous operation for 75 hours, the luminance only attenuates from its initial value (1000 cd m⁻²) to approximately 670 cd m⁻² for PBFDO-based device; whereas ITO-based device can only sustain illumination for about 4 h before reaching this level of luminance. Moreover, ITO-based devices exhibit further luminance degradation to approximately 630 cd m⁻² after continuous operation for about 43 h. Therefore, the

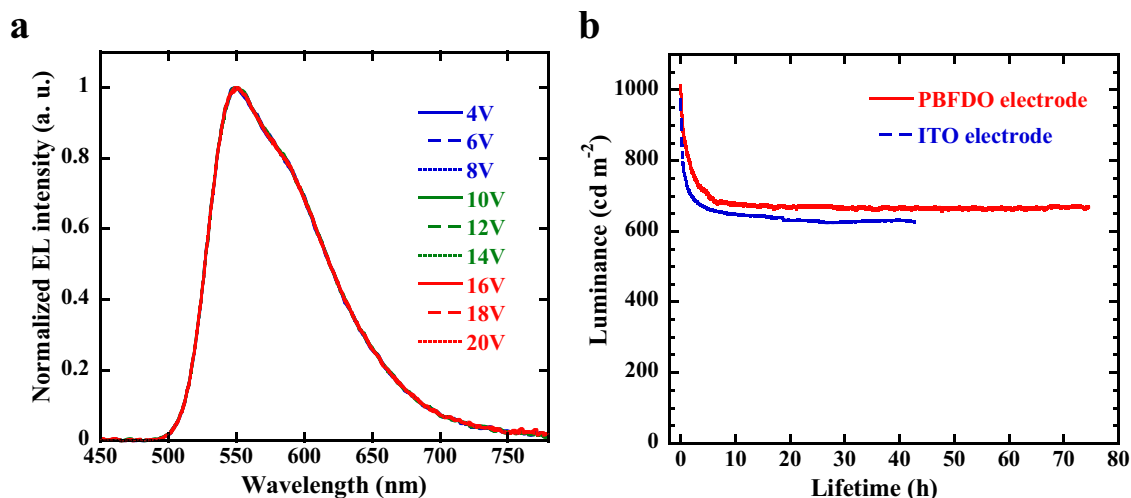


Fig. 8 | Device stability testing. **a** EL spectral stability of OLED devices, utilizing a 25 nm thickness PBFDO electrode, under a driving voltage range of 4–20 V. **b** Luminance-time curve of OLED devices based on PBFDO electrode and ITO electrode under the initial luminance of 1000 cd m^{-2} .

stability of device based on PBFDO electrode is comparable to that observed in device based on ITO electrode.

Finally, the blue OLED was fabricated by employing a PBFDO electrode and the blue light-emitting poly(9,9-dioctyl-2,7-fluorene-co-3,7-dibenzothiophene-S,S-dioxide) (PFSO10), as illustrated in Supplementary Fig. 8 and Table 2 showcasing the corresponding device data. The device based on the PBFDO electrode exhibits a vibrant blue luminescence and demonstrates comparable V_{th} (~ 3.0 V) and LE_{max} (~ 2.5 cd A^{-1}) to those of ITO electrode (Table 2).

Methods

Materials

The conducting solution PBFDO and blue fluorescent polymer (PFSO10) were provided by Dongguan Volt-Amp Optoelectronics Technology Co., Ltd., while PEDOT: PSS (PH 4083) and Super Yellow (SY) were obtained from Heraeus and Sigma Aldrich, respectively. The glass substrate and PEN substrate were purchased from Luoyang Guluo glass Co., LTD and Teijin Limited, respectively.

Device preparation

The glass substrates were sequentially cleaned in an ultrasonic bath containing acetone, detergent, deionized water, and isopropanol. The modified PBFDO solution was prepared by combining n-butanol with PBFDO mother liquor at a volume ratio of 1:2. Prior to spin coating on the glass substrate, the modified PBFDO solution was filtered using a hydrophilic PTFE membrane and then heated at 120 °C for 10 min to eliminate any residual solvent in the film. Multiple spin coatings were employed to achieve PBFDO films of varying thicknesses. Before applying PEDOT:PSS coating onto the PBFDO film, it underwent ethanol washing followed by placement on a heating table at 120 °C for 15 min. Subsequently, a chlorobenzene solution containing SY with a concentration of 6 mg mL^{-1} was spin coated to form a luminescent layer measuring approximately 70 nm in thickness, which was further heated on a heating table at 100 °C for 10 min. Afterwards, the device was transferred into a vacuum evaporation glove box where sequential steam deposition of CsF (1 nm) and Al (100 nm) took place. The identical procedure is employed for the fabrication of flexible devices based on the polyethylene naphthalate (PEN) substrate. The preparation of blue OLED also adopts similar preparation procedure. As testing occurred under ambient conditions, packaging of the device preceded its evaluation.

Characterization

The conductive solution's freezing point and viscosity temperature curves were measured using a differential scanning calorimeter (DSC3, Mettler

Toledo) and a rheometer (MCR702, Anton Paar), respectively. The PBFDO film's thickness and transmittance were determined using a step meter (Dektax XT, Bruker) and UV-Vis-NIR absorption spectrometer (UH4150, Hatachi), respectively. An ellipsometer (SV-VE, Eoptics) was used to measure the refractive index of the PBFDO film. Atomic force microscopy (AFM, Cypher S, Asylum Research) was employed to determine the surface roughness and surface potential of thin films. Fourier Transform infrared (FTIR, Frontier, Perkin Elmer) provided information on the Fourier Transform infrared spectroscopy of the solution and film. Ultraviolet photoelectron spectroscopy (UPS, ESCALAB XI+, Thermo Fisher) measured its work function, the test sample consists of a 65 nm PBFDO thin film deposited on a glass substrate and subsequently subjected to thermal annealing prior to its direct utilization for testing purposes. X-ray diffraction (XRD, Empyrean) provided insight into the crystallization properties of these films. A four-probe resistivity tester (HPS2662, Helprss) was used to measure both surface resistance and conductivity of the film. The luminance-current-voltage curves for devices were obtained using a color luminance meter (CS200, Konica Minolta) by equipping with an active meter (2450, Keithly). Electroluminescence spectra for devices were collected by the fiber optic spectrometer (USB2000+, Ocean Optics).

Data availability

The data that support the findings of this study are available from the corresponding author upon reasonable request.

Received: 4 February 2024; Accepted: 14 June 2024;

Published online: 24 June 2024

References

- Song, H. et al. Water stable and matrix addressable OLED fiber textiles for wearable displays with large emission area. *NPJ Flex. Electron.* **6**, 66 (2022).
- Choi, S. et al. Multi-directionally wrinkle-able textile OLEDs for clothing-type displays. *NPJ Flex. Electron.* **4**, 33 (2020).
- Maasoumi, F. et al. An external quantum efficiency of >20% from solution-processed poly(dendrimer) organic light-emitting diodes. *NPJ Flex. Electron.* **2**, 27 (2018).
- Sun, P., Liu, D., Zhu, F. & Yan, D. An efficient solid-solution crystalline organic light-emitting diode with deep-blue emission. *Nat. Photon.* **17**, 264–272 (2023).
- Nam, M. et al. Highly reliable and stretchable OLEDs based on facile patterning method: toward stretchable organic optoelectronic devices. *NPJ Flex. Electron.* **8**, 17 (2024).

6. Suresh, S. M. et al. A deep-blue-emitting heteroatom-doped MR-TADF nonacene for high-performance organic light-emitting diodes. *Angew. Chem. Int. Ed.* **62**, e202215522 (2023).
7. Yoo, J., Li, S., Kim, D. H., Yang, J. & Choi, M. K. Materials and design strategies for stretchable electroluminescent devices. *Nanoscale Horiz.* **7**, 801–821 (2022).
8. Yin, H., Zhu, Y., Youssef, K., Yu, Z. & Pei, Q. Structures and materials in stretchable electroluminescent devices. *Adv. Mater.* **34**, e2106184 (2022).
9. Yu, Z. et al. Highly flexible silver nanowire electrodes for shape-memory polymer light-emitting diodes. *Adv. Mater.* **23**, 664–668 (2011).
10. Zhou, H. et al. Graphene-based intrinsically stretchable 2D-contact electrodes for highly efficient organic light-emitting diodes. *Adv. Mater.* **34**, e2203040 (2022).
11. Kim, J.-H. & Park, J.-W. Intrinsically stretchable organic light-emitting diodes. *Sci. Adv.* **7**, eabd9715 (2021).
12. Liu, W. et al. High-efficiency stretchable light-emitting polymers from thermally activated delayed fluorescence. *Nat. Mater.* **22**, 737–745 (2023).
13. Han, S. J., Zhou, H., Kwon, H., Woo, S.-J. & Lee, T.-W. Achieving low-voltage operation of intrinsically-stretchable organic light-emitting diodes. *Adv. Funct. Mater.* **33**, 2211150 (2023).
14. Kim, N. et al. Highly conductive PEDOT:PSS nanofibrils induced by solution-processed crystallization. *Adv. Mater.* **26**, 2268–2272 (2014). 2109.
15. He, H. et al. Biocompatible conductive polymers with high conductivity and high stretchability. *ACS Appl. Mater. Interfaces* **11**, 26185–26193 (2019).
16. Jiang, Y. et al. Topological supramolecular network enabled high-conductivity, stretchable organic bioelectronics. *Science* **375**, 1411–1417 (2022).
17. Zhang, Z. et al. High-brightness all-polymer stretchable LED with charge-trapping dilution. *Nature* **603**, 624–630 (2022).
18. Tang, H. et al. A solution-processed n-type conducting polymer with ultrahigh conductivity. *Nature* **611**, 271–277 (2022).
19. Ke, Z. et al. Highly conductive and solution-processable n-doped transparent organic conductor. *J. Am. Chem. Soc.* **145**, 3706–3715 (2023).
20. Tang, H. et al. A solution-processed n-type conducting polymer without side chains formed via nonmetal-participated polymerization and in situ n-doping. *CCS Chem.* **5**, 2534–2544 (2023).
21. Xiang, Z., Chu, C., Xie, H., Xiang, T. & Zhou, S. Multifunctional thermoplastic polyurea based on the synergy of dynamic disulfide bonds and hydrogen bond cross-links. *ACS Appl. Mater. Interfaces* **13**, 1463–1473 (2021).
22. Zehentbauer, F. M. & Kiefer, J. Molecular solution behaviour of an intermediate biofuel feedstock: acetone–butanol–ethanol (ABE). *ChemPhysChem* **16**, 3846–3858 (2015).
23. Yaseen, S. A., Undre, P. B., Saif, F. A., Patil, S. S. & Khirade, P. W. Dielectric and FTIR studies on the hydrogen bonded binary system of ester and alcohol. *Ferroelectrics* **519**, 49–60 (2017).
24. Wong, D. B. et al. Water dynamics in water/DMSO binary mixtures. *J. Phys. Chem. B* **116**, 5479–5490 (2012).
25. Lu, C. & Chen, X. All-temperature flexible supercapacitors enabled by antifreezing and thermally stable hydrogel electrolyte. *Nano Lett.* **20**, 1907–1914 (2020).
26. Kim, K.-T. et al. High performance β -Ga₂O₃ Schottky barrier transistors with large work function TMD gate of NbS₂ and TaS₂. *Adv. Funct. Mater.* **31**, 2010303 (2021).
27. Ji, Q. et al. Metallic vanadium disulfide nanosheets as a platform material for multifunctional electrode applications. *Nano Lett.* **17**, 4908–4916 (2017).
28. Kim, J. H. et al. Work function variation of MoS₂ atomic layers grown with chemical vapor deposition: the effects of thickness and the adsorption of water/oxygen molecules. *Appl. Phys. Lett.* **106**, 251606 (2015).
29. Lattyak, C., Gehrke, K. & Vehse, M. Layer-thickness-dependent work function of MoS₂ on metal and metal oxide substrates. *J. Phys. Chem. C.* **126**, 13929–13935 (2022).
30. Han, L., Chen, Z., Huang, T., Ding, H. & Wu, C. Sensitivity enhancement of Ag-ITO-TMDCs-graphene nanostructure based on surface plasmon resonance biosensors. *Plasmonics* **15**, 693–701 (2020).
31. Xu, J. et al. Color tuning in inverted blue light-emitting diodes based on a polyfluorene derivative by adjusting the thickness of the light-emitting layer. *J. Mater. Chem. C.* **3**, 9819–9826 (2015).
32. Xu, J. et al. Near-infrared polymer light-emitting diodes based on an inverted device structure. *J. Mater. Chem. C.* **7**, 12114–12120 (2019).
33. Xu, J. et al. Challenging conventional wisdom: finding high-performance electrodes for light-emitting electrochemical cells. *ACS Appl. Mater. Interfaces* **10**, 33380–33389 (2018).

Acknowledgements

The research described in this paper was financially supported by the National Natural Science Foundation of China (Grant No. 62005043), the open project of State Key Laboratory of Luminescent Materials and Devices, China (Grant No. 2023-skllmcd-14), and the Basic and Applied Basic Research Foundation of Guangdong Province, China (Grant No. 2019A1515110602).

Author contributions

J.X. and L.Y. designed and supervised the project. J.X. constructed the concept, analyzed the data, and prepared the manuscript. K.D. prepared and characterized the device with the assistance of Z.Z., and W.F. F.P. synthesized the PBFDO solution. J.X., K.D., F.F., Z.S., and Y.L. reviewed and edited the manuscript. All authors discussed the results and commented on the manuscript.

Competing interests

The authors declare no competing interests.

Additional information

Supplementary information The online version contains supplementary material available at <https://doi.org/10.1038/s41528-024-00324-0>.

Correspondence and requests for materials should be addressed to Jin Xu or Lei Ying.

Reprints and permissions information is available at <http://www.nature.com/reprints>

Publisher's note Springer Nature remains neutral with regard to jurisdictional claims in published maps and institutional affiliations.

Open Access This article is licensed under a Creative Commons Attribution 4.0 International License, which permits use, sharing, adaptation, distribution and reproduction in any medium or format, as long as you give appropriate credit to the original author(s) and the source, provide a link to the Creative Commons licence, and indicate if changes were made. The images or other third party material in this article are included in the article's Creative Commons licence, unless indicated otherwise in a credit line to the material. If material is not included in the article's Creative Commons licence and your intended use is not permitted by statutory regulation or exceeds the permitted use, you will need to obtain permission directly from the copyright holder. To view a copy of this licence, visit <http://creativecommons.org/licenses/by/4.0/>.

© The Author(s) 2024